


Article

# Influence of Alkali Treatment on Anodized Titanium Alloys in Wollastonite Suspension

Alicja Kazek-Kęsik <sup>1,\*</sup>, Katarzyna Leśniak <sup>1</sup>, Ivan S. Zhidkov <sup>2</sup> , Danila M. Korotin <sup>2,3</sup>,  
Andrey I. Kukhareenko <sup>3</sup>, Seif O. Cholakh <sup>3</sup>, Izabela Kalemba-Rec <sup>4</sup>, Katarzyna Suchanek <sup>5</sup>,  
Ernst Z. Kurmaev <sup>2,3</sup> and Wojciech Simka <sup>1,\*</sup>

<sup>1</sup> Faculty of Chemistry, Silesian University of Technology, B. Krzywoustego Street 6, 44-100 Gliwice, Poland; katarzyna.lesniak94@gmail.com

<sup>2</sup> Institute of Physics and Technology, Ural Federal University, Mira Street 19, Yekaterinburg 620002, Russia; i.s.zhidkov@urfu.ru (I.S.Z.); danila.korotin@gmail.com (D.M.K.); ernst.kurmaev@gmail.com (E.Z.K.)

<sup>3</sup> M.N. Mikheev Institute of Metal Physics, RAS-Ural Division, Kovalevskoj Street 18, Yekaterinburg 620990, Russia; a.i.kukhareenko@urfu.ru (A.I.K.); s.o.cholakh@urfu.ru (S.O.C.)

<sup>4</sup> Faculty of Metals Engineering and Industrial Computer Science, AGH University of Science and Technology, Mickiewicza Avenue 30, 30-059 Krakow, Poland; kalemba@agh.edu.pl

<sup>5</sup> The Henryk Niewodniczanski Institute of Nuclear Physics, Polish Academy of Sciences, Radzikowskiego Street 152, 31-342 Krakow, Poland; ksuchanek@gmail.com

\* Correspondence: alicja.kazek-kesik@polsl.pl (A.K.-K.); wojciech.simka@polsl.pl (W.S.);  
Tel.: +48-32-237-1754 (A.K.-K.); +48-32-237-2605 (W.S.)

Received: 12 July 2017; Accepted: 17 August 2017; Published: 23 August 2017

**Abstract:** The surface modification of titanium alloys is an effective method to improve their biocompatibility and tailor the material to the desired profile of implant functionality. In this work, technologically-advanced titanium alloys—Ti-15Mo, Ti-13Nb-13Zr and Ti-6Al-7Nb—were anodized in suspensions, followed by treatment in alkali solutions, with wollastonite deposition from the powder phase suspended in solution. The anodized samples were immersed in NaOH or KOH solution with various concentrations with a different set of temperatures and exposure times. Based on their morphologies (observed by scanning electron microscope), the selected samples were investigated by Raman and X-ray photoelectron spectroscopy (XPS). Titanate compounds were formed on the previously anodized titanium surfaces. The surface wettability significantly decreased, mainly on the modified Ti-15Mo alloy surface. Titanium alloy compounds had an influence on the results of the titanium alloys' surface modification, which caused the surfaces to exhibit differential physical properties. In this paper, we present the influence of the anodization procedure on alkali treatment effects and the properties of obtained hybrid coatings.

**Keywords:** titanium alloys; plasma electrolytic oxidation; coatings; alkali treatment

## 1. Introduction

In recent years, emerging new metallic alloys have been extensively tested for potential use in implantation and regenerative medicine, with surface modification tailoring to match the biocompatibility and spectrum of desired bio-functionalities [1–3]. The surface of the metallic materials, aimed at bone implantation, is expected to comply with the ossification process. Towards satisfying these demands, various physical, chemical, and electrochemical techniques have been developed to obtain ceramic-type coatings on the metal surface. A plethora of ceramic layer variations with different surface roughness, wettability, chemical and phase composition, number and size of pores have been examined to indicate the surfaces with the most beneficial bioactivities [4,5]. The bioactivity of the ideal

surface should promote the adhesion and well-being of desired human cells (which are biocompatible) while inhibiting microbe population at the same time (bacteriostatic).

Porous oxide layers formed on the metallic biomaterials via plasma electrolytic oxidation (PEO) exhibit beneficial biological properties towards bone tissue formation. Among other applications, the PEO-layer is often applied on the titanium used in the modification of the bone plate for orthopaedic or orthodontic application, part of endoprosthesis or dental implants which are used as long-bearing implants [6]. The porosity and surface roughness can be precisely controlled for these functionalizations by regulating electrochemical parameters during the PEO process [7,8]. The chemical composition of the coatings depends on both the chemical solutions and the substrate to be coated (elements of the substrate forming oxides). Consequently, the PEO process is widely used for the formation of the bioactive and bacteriostatic surface of bone implants. On top of PEO, an additional treatment of the oxide layer by heat or alkali treatment may be carried out to change the physicochemical properties of the layer, such as its phase composition or wettability. Thus, it is possible to design a titanium alloy surface that exhibits desirable physico-chemical and biological properties [9–11].

Selected titanium alloys, such as Ti-xMo, Ti-xTa-xNb-xZr, Ti-xZr-xNb, are considered as promising metallic implants to bone. The novel titanium alloys are characterized by low Young's modulus and biocompatible alloy elements, compared to Ti-6Al-4V alloy, which is routinely used in medicine [12,13]. The titanium alloy surface is often modified by the PEO process in solution with solved compounds, rather than in suspensions. However, bioactive powders, such as hydroxyapatite or wollastonite, are easy to incorporate into the porous oxide layer [14]. Calcium silicate ( $\text{CaSiO}_3$ ) is a potential material for bone tissue regeneration, since it has been proven to be bioactive and degradable [15]. The apatite formation rate on the surface of  $\text{CaSiO}_3$  is found to be even faster than that of the other bio-glasses and glass-ceramics in simulated body fluid (SBF) [16,17].

The aim of the present work is the alkali treatment of anodized vanadium-free titanium alloy surface as a potential method for enhancing metal surface bioactivity, cytocompatibility and antibacterial properties. The porous oxide layers were formed on the Ti-15Mo, Ti-13Nb-13Zr, Ti-6Al-7Nb by plasma electrolytic oxidation in wollastonite suspensions. Anodized samples were immersed in NaOH or KOH solution at various concentrations and various times of treatment to determine the most appropriate conditions for the oxide layers' alkali treatment.

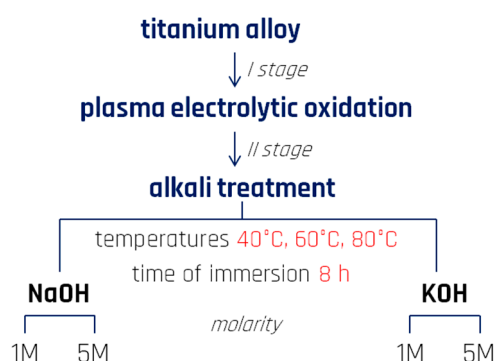
## 2. Materials and Methods

### 2.1. Materials and Procedures of Surface Treatment

Three vanadium-free titanium alloys were chosen for their surface treatment: Ti-15Mo, Ti-13Nb-13Zr, Ti-6Al-7Nb alloys (BIMO Metals, Wroclaw, Poland). The chemical composition of the titanium alloys is presented in Table 1. The metal surface was grinded and etched in solution composed of 1 M HF and 4 M  $\text{H}_2\text{SO}_4$ . Then, the titanium alloys were anodized according to the parameters determined based on our previous results presented in papers [18,19]. A plasma electrolytic oxidation process was carried out in suspensions composed of 0.1 M  $\text{Ca}(\text{H}_2\text{PO}_2)_2$  (Alfa Aesar, Karlsruhe, Germany) and 150 g/dm<sup>3</sup> of wollastonite ( $\text{CaSiO}_3$ ) powder (Carl Jäger, Hilgert, Germany). The voltage limits were 300 V for the Ti-15Mo alloy and 350 V for the Ti-13Nb-13Zr and Ti-6Al-7Nb alloys. The applied voltage and current density were chosen based on our previous investigations, to obtain the best surface morphology after anodization. All of the samples were immersed in various alkali solutions. For each sample, the additional alkali treatment of the anodized surface was carried out. The titanium alloy samples were immersed in 1 M or 5 M of NaOH or KOH solution at 40 °C, 60 °C and 80 °C for 8 h. The titanium alloy surface modification was carried out according to the scheme presented in Figure 1.

**Table 1.** The chemical composition of the titanium alloys (wt %).

Titanium Alloy	Al	Nb	Zr	Ta	Mo	Fe	C	N	H	O	Ti
Ti-6Al-7Nb (TAN)	6.05	6.80	-	0.35	-	0.08	0.04	0.01	0.003	0.11	
Ti-13Nb-13Zr (TNZ)	-	13.30	13.00	-	-	0.08	0.05	0.0009	0.005	0.10	balance
Ti-15Mo (TM)	-	-	-	-	14.73	0.06	0.08	0.016	0.01	0.15	

**Figure 1.** Scheme of titanium alloy surface treatment.

## 2.2. Characterization of the Anodized Surfaces

### 2.2.1. Microstructure, Surface Wettability and Roughness

The microstructure of all of the modified titanium alloys was investigated using a scanning electron microscope (SEM, Hitachi S-3400N, Tokyo, Japan; accelerating voltage = 25 kV). The contact angles were determined using a drop shape analysis system (DSA 10 Mk2, KRÜSS, Hamburg, Germany). Ten drops of 0.20  $\mu$ L ultra-high-purity water at room temperature were used of the measurements for each sample. The surface roughness was measured using a non-contact optical profilometer (Wyko NT9300, Veeco, New York, NY, USA). The surface parameters were determined according to appropriate standard [20].

### 2.2.2. Chemical Composition

XPS measurements and Raman spectroscopy were performed using a high spatial and energy-resolution PHI XPS Versaprobe 5000 spectrometer (ULVAC Physical Electronics, Chanhassen, MN, USA) and a high-resolution Nicolet Almega XR Thermo Electron Corp. (Waltham, MA, USA) system equipped with a 50 mW, 532 nm, frequency-doubled neodymium-yttrium-aluminium-garnet (NdYAG) laser, respectively. The parameters used for investigations were similar to those used in our previous investigations, and details of the measurements are presented in reference [18].

## 3. Results and Discussion

### 3.1. Microstructure of the Modified Titanium Alloy Surfaces

Alkali treatment is an easy method to improve the bioactivity of the oxide layers formed on the titanium alloy surfaces. The formation of additional titanate compounds on the oxide layers can increase the surface area [21]. The amorphous titanate layers facilitate the formation of the apatite-based compounds in physiological solution [22]. During the alkali treatment, a partial dissolution of the titanium oxide occurs, and the amorphous alkali titanate hydrogel is formed on the surface. The amorphous layer can be transformed into crystals by additional heat treatment after surface modification [23].

In our case, titanium alloy samples were anodized in suspensions containing calcium hypophosphite and wollastonite. The best electrochemical parameters for the titanium alloy surfaces'

treatment in the suspensions were determined in our previous works [18,19]. Wollastonite is a bio-compatible compound that enhances osseointegration [24]. The wollastonite particles were incorporated into the oxide layer during the PEO process, and the characteristic particles were observed on the top of the formed layers. Then, the titanium alloy samples were immersed in a variety of alkali solutions for 8 h at a temperature up to 80 °C. The microstructures of the treated titanium alloy surfaces in 1 M NaOH or 1 M KOH are presented in Figures 2 and 3. Immersion in NaOH solution slightly changed the morphology of the anodized sample (Figure 2A–I). The layers were not filled by crystals, on the top of the surfaces' characteristic longitudinal crystals of wollastonite incorporated from the anodizing bath, and fibers were observed. The fibers were formed due to the formation of titanate-based compounds, the corresponding characteristic morphologies of the oxide layers after alkali treatment were presented in papers [25,26]. The anodized TNZ (Ti-13Nb-13Zr) (Figure 3D–F) and TAN (Ti-6Al-7Nb) (Figure 3G–I) alloys soaked in KOH solution resulted in the formation of additional crystals on their surfaces. The layers were cracked when the temperature of the alkali solution was higher than 40 °C, especially on the anodized TNZ sample (Figure 3F). For the anodized T-15Mo (TM) surface (Figure 3I), a single crack was observed, indicated that this coating was the most resistant for cracking in 1 M KOH solution at 80 °C. Interesting results were obtained for the anodized TM alloy samples (Figure 3A–C). The type of the alkali solutions and temperature did not cause cracks in the oxide layer and formation of crystals. In our previous papers, we reported that the oxide layer formed on the TM alloy was more compact than others layers [18,19]. In all probability, the alkali solutions have not penetrated the coatings deeper than that in other oxide layers. The compact oxide layers were more resistant to higher temperatures of alkali solutions.

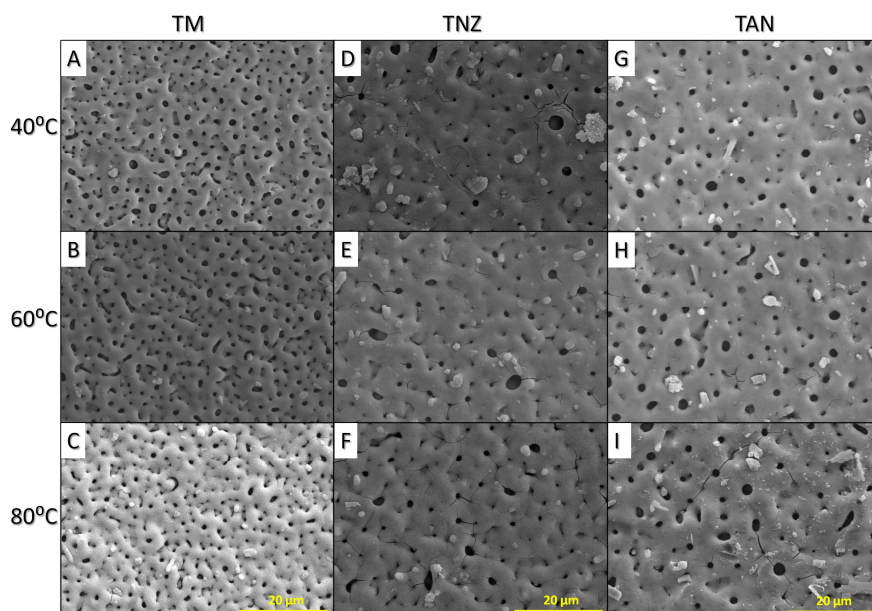


**Figure 2.** SEM images of the titanium TM (A–C), TNZ (D–F), TAN (G–I) alloy samples after anodization and immersion in 1 M NaOH at various temperatures, for 8 h. (TM: T-15Mo; TNZ: Ti-13Nb-13Zr; TAN: Ti-6Al-7Nb.)

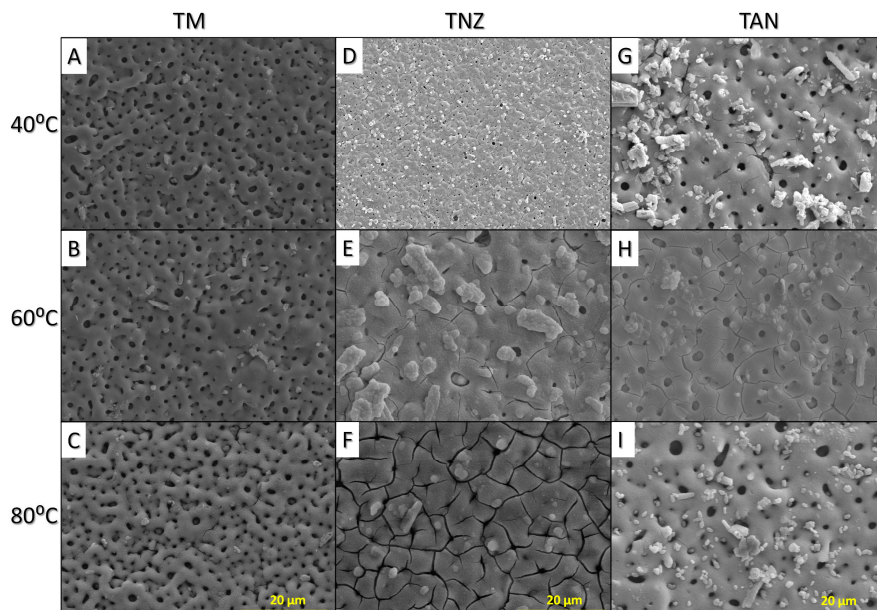


**Figure 3.** SEM images of the titanium TM (A–C), TNZ (D–F), TAN (G–I) alloy samples after anodization and immersion in 1 M KOH at various temperatures, for 8 h.

The microstructures of the coatings soaked in the solutions at higher concentrations of NaOH or KOH (5 M) are presented in Figures 4 and 5. The treatment of the surface in alkali solutions caused the formation of the characteristic nano-fibers of titanate on the oxide layers. No significant changes in layer morphologies were observed on the anodized TM, TNZ, TAN surfaces after immersion in 5 M NaOH at 40 °C (Figure 4A,D,G). Small cracks were observed on the anodized TNZ and TAN samples soaked in KOH at 40 °C (Figure 5A,D,G). Increasing the temperature of the alkali solution resulted in the formation of more prominent cracks in the porous oxide layers. Among these conditions, the 5 M KOH solution caused the highest destruction of the coatings (Figure 5).

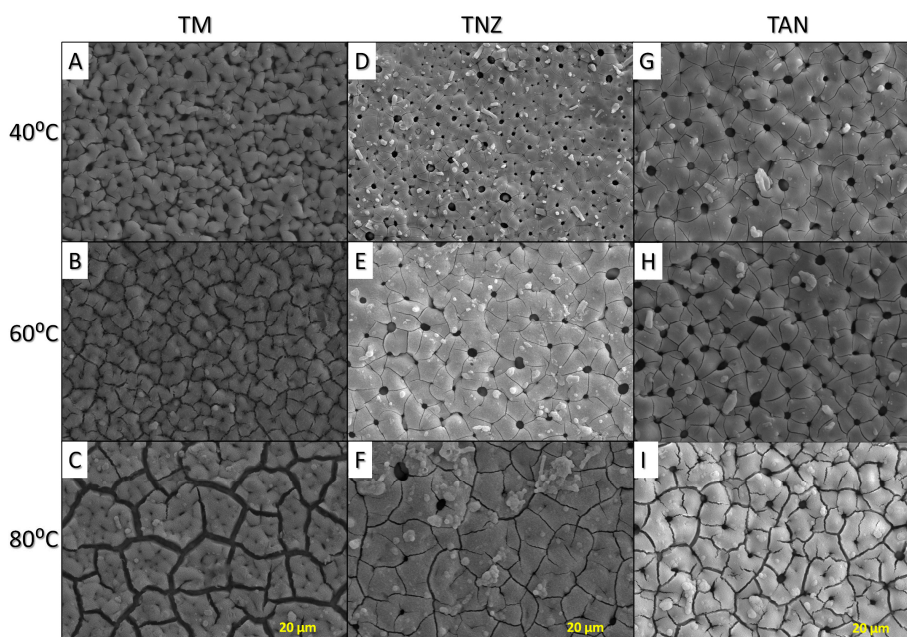


**Figure 4.** SEM images of the titanium TM (A–C), TNZ (D–F), TAN (G–I) alloy samples after anodization and immersion in 5 M NaOH at various temperatures, for 8 h.

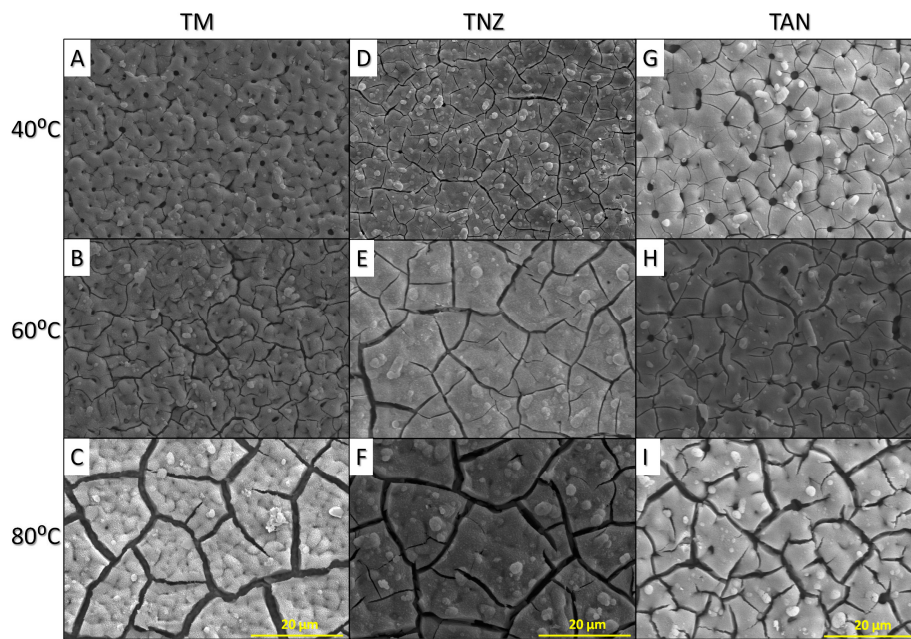


**Figure 5.** SEM images of the titanium TM (A–C), TNZ (D–F), TAN (G–I) alloy samples after anodization and immersion in 5 M KOH at various temperatures, for 8 h.

G.L. Zhao et al. reported that treatment of the PEO layers in solution with concentration of NaOH higher than 5 M, was unfavorable for the layer morphology [27]. However, in our case the oxide layers treated in a higher concentration of NaOH (10 M or 15 M) exhibited a higher ability to form apatite in SBF solution. The cracking of inorganic films might be caused by several factors, one of which is the drying stress related with the temperature and concentration of the alkali solution, and the crystallinity of formed layer. Thicker titanate layers were probably formed in 5 M NaOH or 5 M KOH solution, and layers were more able to crack during drying. Jalota et al. [28] investigated the influences of the drying process on the formation of biomimetic coatings on the titanium alloy surface. They reported that  $\text{CO}_2$  dissolved in deionized water forms carbonic acid ( $\text{H}_2\text{CO}_3$ ), which reacts with sodium ions from the solution, and then  $\text{NaHCO}_3$  is formed. Sodium bicarbonate easily forms sodium carbonate, which might be present in the formed coatings on the top of Ti alloy surface. Carbonate compounds during drying tended to evaporate  $\text{CO}_2$  from the layer, causing layer cracking. It was reported that a crack-free apatite layer was also formed on the Ti alloy surface, when carbonate compounds were removed from the titanate-based coating prior to SBF soaking. Notably, for medical application, the layer formed on the implant surface must not be cracked, due to the possibility of the layer's delamination.

Based on these results, it can be concluded that the KOH solution better penetrated the oxide layers formed on the titanium alloys surface than NaOH solution. The temperature of the alkali solution higher than 60 °C caused cracking of oxide layers. Higher concentration of alkali solution (5 M) also negatively influenced the coatings morphologies. Thus, the anodized titanium alloy samples soaked in 1 M NaOH at 60 °C (Figure 2B,E,H) were chosen for the further investigation. The labels for the chosen samples after anodization and alkali treatments (AT) were TM-AT, TNZ-AT, TAN-AT, while for samples that were only anodized, the labels used were TM-PEO, TNZ-PEO, TAN-PEO, respectively, for each titanium alloy.

### 3.2. Wettability and Surface Roughness

The results of the contact angle and surface roughness measurements of the selected samples are presented in Table 2. The contact angles of the coated samples were much lower compared to the non-coated substrates, probably as a function of the oxide layer formed on substrates. First of all,

the wettability of the surface was changed by the compounds formed on the top of the layers after alkali treatment. The additional compounds and ions adsorbed on the surface during alkali treatment influenced the surface wettability. The contact angle of the TM-AT sample was the lowest, with  $2.3 \pm 0.7^\circ$ , this surface appeared superhydrophilic. For TNZ-AT, surface modification improved the wettability when compared to the non-coated surface, TNZ. The contact angle decreased from  $120 \pm 5.0^\circ$  to  $21.8 \pm 4.6^\circ$  after surface modification. Surface treatment of the TAN caused a decrease in the contact angle from  $51.2 \pm 4.7^\circ$  to  $11.7 \pm 2.7^\circ$ . Depending on the parameters applied during the PEO process, the surface is characterized by different surface roughness parameters. Usually, the highest value of applied voltage causes higher surface roughness, however, to the stage when the outer layer of the coatings might be melt and become smoother. The oxide layers are mainly composed of titanium oxide in the anatase or rutile phase. The nanostructure of  $\text{TiO}_2$  also has an influence on the hydrophilicity [29], which regulates the biological processes for bone cell attachment. In the end, however, the bioactivity and cytocompatibility of the materials also affect the surface topography and the chemical composition of the layer [30]. Most investigations on the dental implant surface focus on mimicking the bone's hierarchical structures due to the formation of bioactive, hydrophilic layers at the micro and/or nanoscale. It was reported that the contact angle of medical dental implants ranges from value near  $0^\circ$  (superhydrophilic) to near  $150^\circ$  (superhydrophobic) [31]. According to Gittens et al., surface wettability affects (i) the adhesion of proteins and other macromolecules, (ii) hard and soft tissue cell interactions, (iii) bacterial adhesion and biofilm formation, and (iv) the rate of the osseointegration in in vivo conditions. Fast processes/reactions on the surface complete within milliseconds. It was reported that dental implant surface should be hydrophilic to enhance adhesion and orientation of selected proteins [32,33].

The formation of porous layers significantly increased the surface roughness, similar observation was reported in paper [34]. Surface treatment slightly changed the titanium alloys surface roughness ( $R_a$ ,  $R_q$ ,  $R_z$ ). The  $R_a$  parameter determined for the TNZ-AT and TAN-AT was approximately similar,  $2.74 \mu\text{m}$  and  $2.37 \mu\text{m}$ , respectively. The maximum height of the roughness ( $R_z$ ) for the TNZ-AT was higher compared to  $R_z$  for TAN-AT. The oxide layer formed on the TNZ-AT was thicker and less uniform, thus the  $R_z$  parameter was higher. The surface roughness was characterized using an optical profilometer, so the characterization of the nanostructures and small sharp pores or cracks might be less precise due to the resolution of the equipment. Thus, the surface roughness was not compared between samples after anodization and samples after anodization and alkali treatment.

**Table 2.** The sample labels, wettability, surface roughness and 3D image of the investigated samples determined by an optical profilometer. (TM: Ti-15Mo; TNZ: Ti-13Nb-13Zr; TAN: Ti-6Al-7Nb; AT: Alkali treatments.)

Sample	Contact Angle/ $^\circ$	Surface Roughness, $\mu\text{m}$		
		$R_a$	$R_q$	$R_z$
TM	$47.6 \pm 5.7$	0.28	0.36	0.30
TM-AT	$2.3 \pm 0.7$	1.08	2.19	309.06
TNZ	$120 \pm 5.0$	0.51	0.63	9.77
TNZ-AT	$21.8 \pm 4.6$	2.74	3.39	168.09
TAN	$51.2 \pm 4.7$	0.30	0.48	1.48
TAN-AT	$11.7 \pm 2.7$	2.37	2.91	92.40

The thicknesses of the oxide layers formed on the titanium alloys were determined in our previously published studies [18,19]. For the anodized TNZ sample, the oxide layer thickness was between  $7.47\text{--}9.30 \mu\text{m}$ , for anodized TAN it was  $5.58\text{--}7.91 \mu\text{m}$ , and for anodized TM it was  $3.40\text{--}4.60 \mu\text{m}$ . The thicknesses of the layers after PEO and alkali treatment were not determined, because the additional treatment of the oxide layer usually does not significantly affect the layer thickness; moreover, the procedure of sample preparation for cross-section analysis may destroy the

thin layer composed of titanate. The thickness of the anodized TM sample was lower compared to others, because the substrate was anodized at lower voltage 300 V, while the TAN and TNZ alloys were anodized at 350 V. Usually, the higher voltage applied during the PEO process leads to increased layer thickness. The applied voltage is also correlated with the surface roughness. Accordingly, the  $R_a$  parameter of the TM-AT sample was lower. The differentiation, proliferation rate, cell mobility, extracellular matrix synthesis, protein synthesis of human osteoblast-like cells MG-63, all depend on the wettability and surface roughness. An investigation on the biocompatibility of the titanium surface with various roughness was evaluated in detail by Martin et al. [35]. It was suggested that surface roughness may determine the phenotypic characteristics of cells in vivo.

### 3.3. Chemical Composition Analysis

After samples immersion in NaOH (or KOH) solutions, structures composed of  $\text{Na}_2\text{TiO}_3$ ,  $\text{Na}_2\text{Ti}_6\text{O}_{13}$ ,  $\text{Na}_4\text{Ti}_5\text{O}_{12}$ ,  $\text{Na}_2\text{Ti}_9\text{O}_{19}$  can be formed. The alkali treatment can be coupled with the other additional techniques for surface treatment, e.g., heat treatment. The mechanisms of the formation of titanate compounds in alkali solution are described in publication [36].

### 3.4. XPS Measurement

The XPS survey spectra of PEO-treated TAN, TM and TNZ alloys are presented in Figure 6. The surface composition determined from these spectra (see Table 3) shows that Na, Ca and Si atoms are incorporated to the surface of these alloys. It can be seen that  $\text{CaSiO}_3$  coatings primarily consist of Na, Ca, Ti, Al, Nb, Mo, Zr and O elements, with  $0.6 \pm 0.2\%$  of Si content. The spectrum for Na 1s overlapped with the Ti Auger line; hence, the position of the Na 1s line could not be precisely defined, and the bond between Na–O or Na–OH could not be recognized with sufficient confidence. However, based on these results, it was clear that compounds containing Na were present on the treated titanium alloy surface.

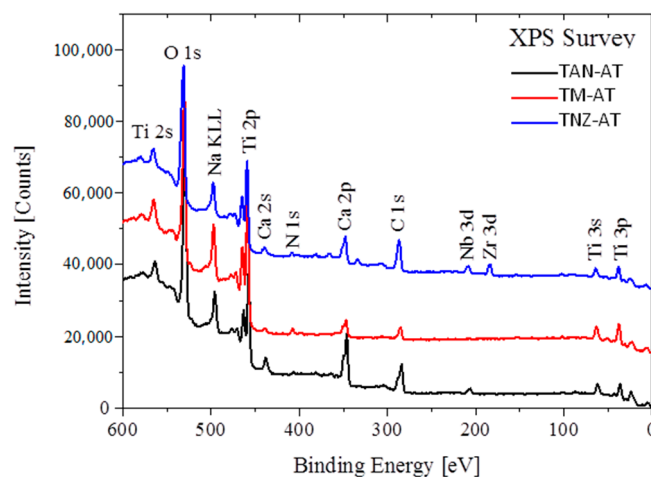


**Figure 6.** XPS (X-ray photoelectron spectroscopy) survey spectra of plasma electrolytic oxidation (PEO)-treated Ti-6Al-7Nb (TAN), Ti-15Mo (TM) and Ti-13Nb-13Zr (TNZ) alloys.

**Table 3.** Surface composition of alkali-treated titanium alloys.

Sample	Concentration, at %								
	Ti	Al	Nb/Mo	Ca	Na	Zr	C	O	Si
TM-AT	17.1	-	0.1	2.4	13.4	-	11.1	55.3	0.6
TNZ-AT	9.5	-	0.5	3.4	6.3	0.9	27.7	50.9	0.8
TAN-AT	9.8	0.3	0.3	5.6	7.5	-	24.6	51.4	0.5



The high-energy resolved XPS Ca 2p, Ti 2p, Si 2p and O 1s spectra of treated Ti alloys are presented in Figure 7a–d. The binding energy of XPS Ca 2p<sup>3/2</sup> peak (at 347.0 eV) is found to be the same for all three alloys and corresponds to the Ca–O bond of CaSiO<sub>3</sub> [37]. The XPS Si 2p peak position could be well fitted at 102.0 eV, relating to Si 2p in CaSiO<sub>3</sub>, but different from that of SiO<sub>2</sub> (at 103.3 eV). The XPS Ti 2p spectra of the coatings show a peak-doublet of Ti 2p<sup>3/2</sup> at 458.6 eV and Ti 2p<sup>1/2</sup> at 464.4 eV, which are binding energies typical for TiO<sub>2</sub> [38]. The XPS O 1s-spectra showed the splitting into two lines corresponding to O–Ti bonds (at 530.2 eV), O–Ca bonds (531.8 eV) and hydroxyl group OH<sup>−</sup> (at 532.8 eV). The contribution of O–Ca bonds is maximal for TAN alloy and reduced in TM and TNZ alloys in correspondence with Ca-concentration (see Table 3).

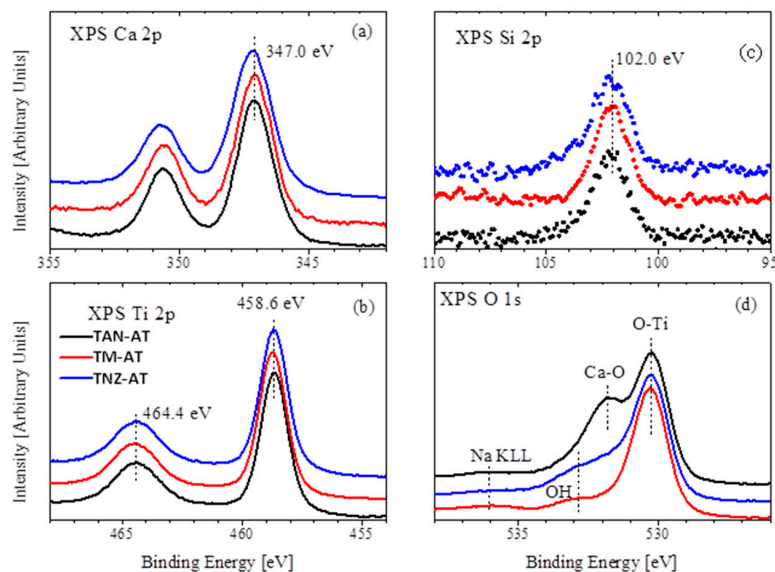


**Figure 7.** XPS (X-ray photoelectron spectroscopy) Ca 2p (a), Ti 2p (b), Si 2p (c) and O 1s (d) of treated Ti-alloys.

XPS valence band spectra (Figure 8) showed that the intensity ratio of Ca 3p/O 2s lines corresponded to Ca/O composition (see Table 3). The top of the valence band for all alloys is found to be very similar and close to that of TiO<sub>2</sub> [39], which means that a corrosion-resistant TiO<sub>2</sub> thin film is formed during PEO treatment. The high-energy structure at 9–14 eV can be related to contribution of OH<sup>−</sup> groups. The appearance of such an active functional group can be favorable for the biocompatibility of treated surfaces; in particular, to fibrinogen adsorption and the enhanced affinity for albumin binding over fibrinogen [40].

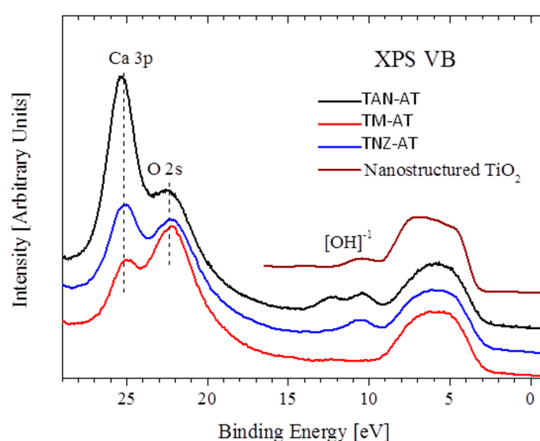


**Figure 8.** XPS valence bands in treated Ti alloys.

### 3.5. Raman Spectroscopy

Figure 9 presents the Raman spectra of anodized titanium alloy samples (red line), and those additionally immersed in NaOH solution (black line). For all of the samples, the bands characteristic for the  $\text{PO}_4^{3-}$  group at  $961\text{ cm}^{-1}$ ,  $430\text{--}450\text{ cm}^{-1}$ ,  $580\text{--}620\text{ cm}^{-1}$ , and  $1030\text{--}1080\text{ cm}^{-1}$  were detected. The signal at  $144\text{ cm}^{-1}$  is characteristic for the crystal form of anatase. The signal at  $156\text{ cm}^{-1}$  was only observed for the TAN-PEO sample (Figure 9C), which is related to  $\text{TiO}_2$ . The bonds with signals near  $2900\text{ cm}^{-1}$  and  $3400\text{ cm}^{-1}$  were recognized as the  $\text{OH}^-$  group. For the TM-PEO sample (Figure 9A, red line) the signals were less intensive compared to the other samples treated by anodization only. It could be concluded that the titanium oxide formed on the TM-PEO sample took an amorphous form rather than crystalline. For the TNZ-PEO sample (Figure 9B, red line), the signals at  $1085\text{ cm}^{-1}$ ,  $1250\text{ cm}^{-1}$ ,  $1320\text{ cm}^{-1}$  and  $1600\text{ cm}^{-1}$  were difficult to annotate to one compound; these signals are probably connected with compounds composed of carbon bonds, such as  $\text{C-O}$ ,  $\text{C=C}$ ,  $\text{C-OH}$ . Some of the calcite might possibly be formed on the treated titanium alloy surface during the immersion in alkali solution. For all of the Raman spectra (spectra with black line on the Figure 9), the signals between  $100\text{--}880\text{ cm}^{-1}$  became broad, with lower intensity. The bond signals observed on the anodized samples between  $1600\text{ cm}^{-1}$  and  $3400\text{ cm}^{-1}$  disappeared. A decreasing of the signals and broad shape near  $280\text{ cm}^{-1}$  and  $456\text{ cm}^{-1}$  are both related to the presence of the titanate phases of  $\text{Ti-O}$  broad in sodium titanate or compounds such as  $\text{H}_3\text{Ti}_3\text{O}_7$ ,  $\text{H}_2\text{Ti}_4\text{O}_9$  [41]. The broad shape of the signals near  $150\text{ cm}^{-1}$ ,  $217\text{ cm}^{-1}$ ,  $650\text{ cm}^{-1}$  and  $880\text{ cm}^{-1}$  may indicate the deformation of the octahedron of  $\text{TiO}_2$  and a changing in the bond length of  $\text{Ti-O}$ .

Bioactive compounds, including titanate, in appropriate concentration might stimuli bone cell proliferation and, in the case of mesenchymal cells, their differentiation, proliferation and mineralization [42]. It was reported that wollastonite and pseudowollastonite show a high bioactivity in the simulated body environment [43]. Thus, this kind of ceramic is considered as an excellent material for formation scaffolds and other composite materials which offers advancements in bone repair [24,44]. However, in our previous paper, we showed that wollastonite particles can be successfully incorporated into the porous oxide layer during the anodizing process [18,19]. Osteoconduction and osseousubstitution properties of the materials can be enhanced by surface immersion in solutions such as trimethanol aminomethane, sodium or potassium hydroxide to obtain a negatively charged surface [17]. Calcium ions attracted a functional group more easily and created apatite crystals. The chemical and phase composition, as well as the shape of crystals, depend on titanate-oxide layer binding. Due to the various composition of the titanium alloys, the chemical composition of the formed oxide layer after anodization is expected to be different, and thus the results of additional alkali treatment will be also different.

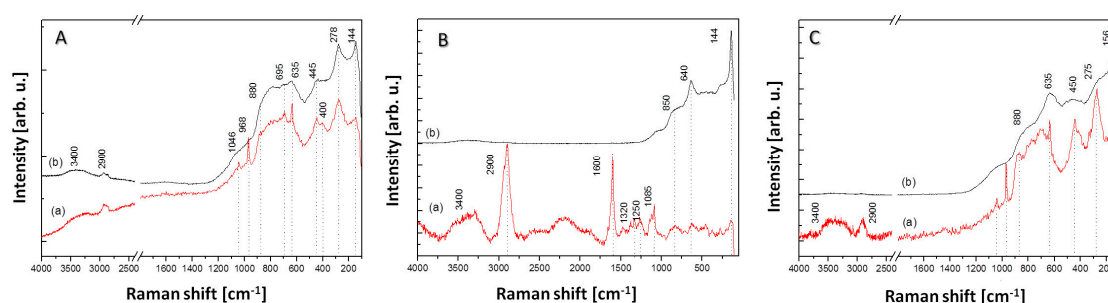


**Figure 9.** Raman spectra of (A) TM-alkali treatments (AT); (B) TNZ-AT; (C) TAN-AT samples. (Red line: Anodized titanium alloy samples; Black line: Immersed in NaOH solution.)

## 4. Conclusions

In our study, the porous oxide layer formed on the titanium was achieved using the alkali solutions. In this case, the optimal condition for the oxide layers' treatment was a solution containing

1 M NaOH at temperature of 60 °C for 8 h. On the oxides, characteristic flakes were formed, due to the formation of the titanate compounds. The highest concentration of sodium was determined for the treated Ti-15Mo surface. The alkali treatment of anodized Ti-13Nb-13Zr and Ti-6Al-7Nb alloy caused the formation of Na-based compounds to be similar. Surface treatment strongly decreased the water contact angle of Ti alloys, and most hydrophilic properties exhibited coated Ti-15Mo. However, the highest influence of alkali treatment on physical properties was determined for the anodized Ti-13Nb-13Zr alloy. The surface morphology and chemical composition of the alkali-treated oxide layer may exhibit high bioactivity. The proposed techniques for the titanium alloy surface modification present a simple way to obtain a functional surface for biomedical applications.

**Acknowledgments:** This work was supported by the Polish Ministry of Science and Education under research project No. IP 2012 0459 72 and by the Silesian University of Technology, Gliwice, Poland, as a Rector's grant. XPS measurements were supported by the Russian Foundation for Basic Research (Project 17-02-00005 and 16-32-00006), Government of Russian Federation (Act 211, agreement No. 02.A03.21.0006) and President of Russia Grant No. MK-1145.2017.2.

**Author Contributions:** A.K.-K. and W.S. conceived and designed the experiments; A.K.-K. performed the experiments; A.K.-K. and I.S.Z. and D.M.K and A.I.K and S.O.C. and E.Z.K. analyzed the data; K.L. and I.K.-R. and K.S. contributed reagents/materials/analysis tools; A.K.-K. and E.Z.K. and W.S. wrote the paper.

**Conflicts of Interest:** The authors declare no conflict of interest.

## References

1. Prasad, S.; Ehrensberger, M. Biomaterial properties of titanium in dentistry. *J. Oral Biosci.* **2015**, *57*, 192–199. [[CrossRef](#)]
2. Cordeiro, J.M.; Barão, V.A.R. Is there scientific evidence favoring the substitution of commercially pure titanium with titanium alloys for the manufacture of dental implants? *Mater. Sci. Eng. C* **2017**, *71*, 1201–1215. [[CrossRef](#)] [[PubMed](#)]
3. Mahapatro, A. Bio-functional nano-coatings on metallic biomaterials. *Mater. Sci. Eng. C* **2015**, *55*, 227–251. [[CrossRef](#)] [[PubMed](#)]
4. Chen, Q.; Thouas, G.A. Metallic implant biomaterials. *Mater. Sci. Eng. R Rep.* **2015**, *87*, 1–57. [[CrossRef](#)]
5. Mani, G. Surface Properties and Characterization of Metallic Biomaterials. In *Surface Coating and Modification of Metallic Biomaterials*, 1st ed.; Wen, C., Ed.; Elsevier: Amsterdam, The Netherlands, 2016; Volume 3, pp. 61–77.
6. Kaluderović, M.R.; Schreckenbach, J.P.; Graf, H.L. Titanium dental implant surfaces obtained by anodic spark deposition—From the past to the future. *Mater. Sci. Eng. C* **2016**, *69*, 1429–1441. [[CrossRef](#)] [[PubMed](#)]
7. Rokosz, K.; Hryniewicz, T.; Matýsek, D.; Raaen, S.; Valiček, J.; Dudek, Ł.; Harničárová, M. SEM, EDS and XPS analysis of the coatings obtained on titanium after plasma electrolytic oxidation in electrolytes containing copper nitrate. *Materials* **2016**, *9*, 318. [[CrossRef](#)] [[PubMed](#)]
8. Rokosz, K.; Hryniewicz, T.; Malorny, W. Characterization of coatings created on selected titanium alloys by plasma electrolytic oxidation. *Adv. Mater. Sci.* **2016**, *6*, 5–16. [[CrossRef](#)]
9. Lee, B.H.; Kim, Y.D.; Shin, J.H.; Lee, K.H. Surface modification by alkali and heat treatments in titanium alloys. *J. Biomed. Mater. Res.* **2002**, *61*, 466–473. [[CrossRef](#)] [[PubMed](#)]
10. Yavari, A.S.; Ahmadi, S.M.; Stok, J.; Wauthle, R.; Riemsdag, A.C.; Janssen, M.; Schrooten, J.; Weinans, H.; Zadpoor, A.A. Effects of bio-functionalizing surface treatments on the mechanical behavior of open porous titanium biomaterials. *J. Mech. Behav. Biomed. Mater.* **2014**, *36*, 109–119. [[CrossRef](#)] [[PubMed](#)]
11. Yan, Z.; Wu, M.; Qin, H.; He, Y.; Yu, X.; Chen, L. ZrO<sub>2</sub>/TiO<sub>2</sub> films prepared by plasma electrolytic oxidation and a post treatment. *Surf. Coat. Technol.* **2017**, *309*, 331–336. [[CrossRef](#)]
12. Bai, Y.; Deng, Y.; Zheng, Y.; Li, Y.; Zhang, R.; Lv, Y.; Zhao, Q.; Wei, S. Characterization, corrosion behavior, cellular response and in vivo bone tissue compatibility of titanium–niobium alloy with low Young's modulus. *Mater. Sci. Eng. C* **2016**, *59*, 565–576. [[CrossRef](#)] [[PubMed](#)]
13. Correa, D.R.N.; Vicente, F.B.; Donato, T.A.G.; Arana-Chavez, V.E.; Buzalaf, M.A.R.; Grandini, C.R. The effect of the solute on the structure, selected mechanical properties, and biocompatibility of Ti–Zr system alloys for dental applications. *Mater. Sci. Eng. C* **2014**, *34*, 354–359. [[CrossRef](#)] [[PubMed](#)]

14. Wu, C.; Ramaswamy, Y.; Boughton, P.; Zreiqat, H. Improvement of mechanical and biological properties of porous CaSiO<sub>3</sub> scaffolds by poly(D,L-lactic acid) modification. *Acta Biomater.* **2008**, *4*, 343–353. [[CrossRef](#)] [[PubMed](#)]
15. Sadjadia, M.S.; Ebrahimia, H.R.; Meskinfam, M.; Zare, K. Silica enhanced formation of hydroxyapatite nanocrystals in simulated body fluid (SBF) at 37 °C. *Mater. Chem. Phys.* **2011**, *130*, 67–71. [[CrossRef](#)]
16. Siriphannon, P.; Kameshima, Y.; Yasumori, A.; Okada, K.; Hayashi, S. Formation of hydroxyapatite on CaSiO<sub>3</sub> powders in simulated body fluid. *J. Eur. Ceram. Soc.* **2002**, *22*, 511–520. [[CrossRef](#)]
17. Liu, X.; Ding, C.; Chu, P.K. Mechanism of apatite formation on wollastonite coatings in simulated body fluid. *Biomaterials* **2004**, *25*, 1755–1761. [[CrossRef](#)] [[PubMed](#)]
18. Kazek-Kęsik, A.; Dercz, G.; Kalemba, I.; Suchanek, K.; Kukhareenko, A.I.; Korotin, D.M.; Michalska, J.; Krzakała, A.; Piotrowski, J.; Kurmaev, E.Z.; et al. Surface characterisation of Ti–15Mo alloy modified by a PEO process in various suspensions. *Mater. Sci. Eng. C* **2014**, *39*, 259–272. [[CrossRef](#)] [[PubMed](#)]
19. Kazek-Kęsik, A.; Dercz, G.; Suchanek, K.; Kalemba-Rec, I.; Piotrowski, J.; Simka, W. Biofunctionalization of Ti–13Nb–13Zr alloy surface by plasma electrolytic oxidation. Part I. *Surf. Coat. Technol.* **2015**, *276*, 59–69. [[CrossRef](#)]
20. ISO 4287:1999 Geometrical Product Specification (GPS)—Surface Texture: Profile Methods—Terms, Definitions and Surface Texture Parameters. Available online: <https://www.iso.org/standard/10132.html> (accessed on 18 August 2017).
21. Wu, J.M.; Song, X.M.; Yan, M. Alkaline hydrothermal synthesis of homogeneous titania microspheres with urchin-like nanoarchitectures for dye effluent treatments. *J. Hazard. Mater.* **2011**, *194*, 338–344. [[CrossRef](#)] [[PubMed](#)]
22. Kokubo, T.; Yamaguchi, S. Bioactive titanate layers formed on titanium and its alloys by simple chemical and heat treatments. *Open Biomed. Eng. J.* **2015**, *9*, 29–41. [[CrossRef](#)] [[PubMed](#)]
23. Lee, K.; Yoo, D. Large-area sodium titanate nanorods formed on titanium surface via. NaOH alkali treatment. *Arch. Metall. Mater.* **2015**, *60*, 1371–1374. [[CrossRef](#)]
24. Sainitya, R.; Sriram, M.; Kalyanaraman, V.; Dhivya, S.; Saravanan, S.; Vairamani, M.; Sastry, T.P.; Selvamurugan, N. Scaffolds containing chitosan/carboxymethyl cellulose/mesoporous wollastonite for bone tissue engineering. *Int. J. Biol. Macromol.* **2015**, *80*, 481–488. [[CrossRef](#)] [[PubMed](#)]
25. Kim, S.Y.; Kim, Y.L.; Park, L.S.; Jin, G.C.; Bae, T.S.; Lee, M.H. Effect of alkali and heat treatments for bioactivity of TiO<sub>2</sub> nanotubes. *Appl. Surf. Sci.* **2014**, *321*, 412–419. [[CrossRef](#)]
26. Park, S.Y.; Jo, C.I.; Choe, H.C.; Brantley, W.A. Hydroxyapatite deposition on micropore-formed Ti-Ta-Nb alloys by plasma electrolytic oxidation for dental applications. *Surf. Coat. Technol.* **2016**, *294*, 15–20. [[CrossRef](#)]
27. Zhao, G.L.; Xiao, L.; Zhong, B.; Wu, S.S.; Song, L.; Wen, G.W. Effect of alkali treatments on apatite formation of microarc-oxidized coating on titanium alloy surface. *Trans. Nonferrous Met. Soc. China* **2015**, *25*, 1151–1157. [[CrossRef](#)]
28. Jalota, S.; Bhaduri, S.; Bhaduri, S.B. A protocol to develop crack-free biomimetic coatings on Ti6Al4V substrates. *J. Mater. Res.* **2007**, *22*, 1593–1600. [[CrossRef](#)]
29. Baoe, L.; Jun, L.; Chunyong, L.; Haipeng, L.; Litong, G.; Shimin, L.; Hongshui, W. Surface roughness and hydrophilicity of titanium after anodic oxidation. *Rare Met. Mater. Eng.* **2016**, *45*, 858–862.
30. Lampin, M.; Warocquier-Clérout, R.; Legris, C.; Degrange, M.; Sigot-Luizard, M. Correlation between substratum roughness and wettability, cell adhesion, and cell migration. *J. Biomed. Mater. Res.* **1997**, *36*, 99–108. [[CrossRef](#)]
31. Gittens, R.A.; Scheideler, L.; Rupp, F.; Hyzy, S.L.; Geis-Gerstorfer, J.; Schwartz, Z.; Boyan, B.D. A review on the wettability of dental implant surfaces II: Biological and clinical aspects. *Acta Biomater.* **2014**, *10*, 2907–2918. [[CrossRef](#)] [[PubMed](#)]
32. Song, W.H.; Jun, Y.K.; Han, Y.; Hong, S.H. Biomimetic apatite coatings on micro-arc oxidized titania. *Biomaterials* **2004**, *25*, 3341–3349. [[CrossRef](#)] [[PubMed](#)]
33. Matykina, E.; Arrabal, R.; Skeldon, P.; Thompson, G.E. Transmission electron microscopy of coatings formed by plasma electrolytic oxidation of titanium. *Acta Biomater.* **2009**, *5*, 1356–1366. [[CrossRef](#)] [[PubMed](#)]
34. Padiál-Molina, M.; Galindo-Moreno, P.; Fernández-Barbero, J.E.; O’Valle, F.; Jódar-Reyes, A.B.; Ortega-Vinuesa, J.L.; Ramón-Torregrosa, P.J. Role of wettability and nanoroughness on interactions between osteoblast and modified silicon surfaces. *Acta Biomater.* **2011**, *7*, 771–778. [[CrossRef](#)] [[PubMed](#)]

35. Martin, J.Y.; Schwartz, Z.; Hummert, T.W.; Schraub, T.M.; Simpson, J.; Lankford, J.; Dean, D.D.; Cochran, D.L.; Boyan, B.D. Effect of titanium surface roughness on proliferation, differentiation, and protein synthesis of human osteoblast-like cells (MG63). *J. Biomed. Mater. Res.* **1995**, *29*, 389–401. [[CrossRef](#)] [[PubMed](#)]
36. Jokanovic, V.; Vilotijevic, M.; Jokanovic, B.; Jenko, M.; Anzel, I.; Stamenkovic, D.; Lazic, V.; Rudolf, R. Investigations of corrosion on the surface of titanium substrate caused by combined alkaline and heat treatment. *Corros. Sci.* **2014**, *82*, 180–190. [[CrossRef](#)]
37. Zhang, W.; Du, K.; Yan, C.; Wang, F. Preparation and characterization of a novel Si-incorporated ceramic film on pure titanium by plasma electrolytic oxidation. *Appl. Surf. Sci.* **2008**, *254*, 5216–5223. [[CrossRef](#)]
38. Wagner, C.D.; Riggs, W.M.; Davis, L.E.; Moulder, J.E.; Mulenger, G.E. *Handbook of X-ray Photoelectron Spectroscopy*, 1st ed.; Perkin Elmer Corp.: Eden Prairie, MN, USA, 1979.
39. Fusi, M.; Maccallini, E.; Caruso, T.; Casari, C.S.; Li Bassi, A.; Bottani, C.E.; Rudolf, P.; Prince, K.C.; Agostino, R.G. Surface electronic and structural properties of nanostructured titanium oxide grown by pulsed laser deposition. *Surf. Sci.* **2011**, *605*, 333–340. [[CrossRef](#)]
40. Thevenot, P.; Hu, W.; Tang, L. Surface chemistry influences implant biocompatibility. *Curr. Top. Med. Chem.* **2008**, *8*, 270–280. [[PubMed](#)]
41. Nguyen-Phan, T.D.; Pham, V.H.; Kim, E.J.; Oh, E.S.; Hur, S.H.; Chung, J.S.; Lee, B.; Shin, E.W. Reduced graphene oxide–titanate hybrids: Morphologic evolution by alkali-solvothermal treatment and applications in water purification. *Appl. Surf. Sci.* **2012**, *258*, 4551–4557. [[CrossRef](#)]
42. Nebe, J.B.; Müller, L.; Lüthen, F.; Ewald, A.; Bergemann, C.; Conforto, E.; Müller, F.A. Osteoblast response to biomimetically altered titanium surfaces. *Acta Biomater.* **2008**, *4*, 1985–1995. [[CrossRef](#)] [[PubMed](#)]
43. De Aza, P.N.; Luklinska, Z.B.; Anseau, M.R.; Hector, M.; Guitián, F.; De Aza, S. Reactivity of a wollastonite–tricalcium phosphate bioeutectic ceramic in human parotid saliva. *Biomaterials* **2000**, *21*, 1735–1741. [[CrossRef](#)]
44. Shao, H.; He, Y.; Fu, J.; He, D.; Yang, X.; Xie, J.; Yao, C.; Ye, J.; Xu, S.; Gou, Z. 3D printing magnesium-doped wollastonite/ $\beta$ -TCP bioceramics scaffolds with high strength and adjustable degradation. *J. Eur. Ceram. Soc.* **2016**, *35*, 1495–1503. [[CrossRef](#)]



© 2017 by the authors. Licensee MDPI, Basel, Switzerland. This article is an open access article distributed under the terms and conditions of the Creative Commons Attribution (CC BY) license (<http://creativecommons.org/licenses/by/4.0/>).